Nitrate attenuation in low-permeability sediments based on isotopic and microbial analyses

Article *in* Science of The Total Environment · March 2018

DOI: 10.1016/j.scitotenv.2017.11.039

7 authors, including:

Yuexia Wu
Peking University
12 PUBLICATIONS **155** CITATIONS
SEE PROFILE

Xiqing Li
Peking University
46 PUBLICATIONS **1,372** CITATIONS
SEE PROFILE

Chunmiao Zheng
Southern University of Science and Technology
257 PUBLICATIONS **6,084** CITATIONS
SEE PROFILE

Science of the Total Environment 618 (2018) 15–25

Contents lists available at ScienceDirect

Science of the Total Environment

journal homepage: www.elsevier.com/locate/scitotenv

Nitrate attenuation in low-permeability sediments based on isotopic and microbial analyses

Yuexia Wu [a,b], Ligang Xu [a,*], Sai Wang [c], Zhenglu Wang [d], Jianying Shang [e], Xiqing Li [d], Chunmiao Zheng [f]

[a] Key Laboratory of Watershed Geographic Sciences, Nanjing Institute of Geography & Limnology, Chinese Academy of Sciences, 73 East Beijing Road, 210008 Nanjing, PR China
[b] Institute of Water Sciences, College of Engineering, Peking University, No. 5 Yiheyuan Road, 100871 Beijing, PR China
[c] Center for Hydrogeology and Environmental Geology, China Geological Survey, No. 1305 Qiyi Road, North District, Baoding, Hebei Province, PR China
[d] College of Urban and Environmental Science, Peking University, 100871 Beijing, PR China
[e] College of Resources & Environmental Science, China Agricultural University, 100193 Beijing, PR China
[f] School of Environmental Science and Engineering, South University of Science and Technology, 518025 Shenzhen, PR China

HIGHLIGHTS

- The LPS was demonstrated to have a high nitrate reduction potential.
- Denitrification was identified to be the main pathway of nitrate attenuation.
- Chemlithotrophic denitrification plays a significant role in nitrate attenuation in the LPS.

GRAPHICAL ABSTRACT

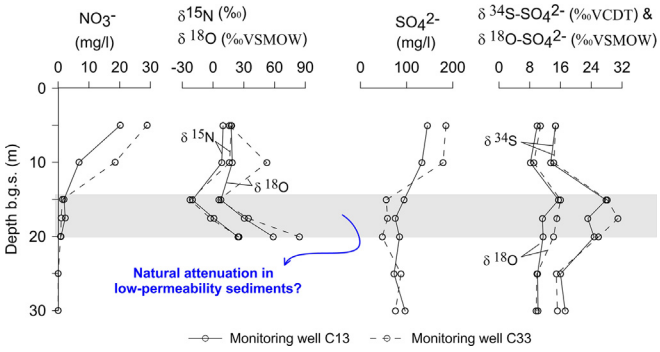

ARTICLE INFO

Article history:
Received 16 August 2017
Received in revised form 3 November 2017
Accepted 3 November 2017
Available online xxxx

Editor: F.M. Tack

Keywords:
Nitrate attenuation
Low-permeability sediments
Microbial diversity
Isotopic analyses
Sulfate reduction

ABSTRACT

This study investigated nitrate attenuation in low-permeability sediments (LPS) in a multi-layer aquifer by integrating hydrochemical, isotopic and microbiological molecular techniques in a field site. In the meantime, the overlying high-permeability sediment (HPS) was also examined on the nitrate attenuation for the sake of comparison. Additionally, laboratory flow-through experiments were conducted to assess the overall nitrate reduction rate in the two types of sediment. The $\delta^{15}N\text{-}NO_3^-$ and $\delta^{34}S\text{-}SO_4^{2-}$ values were more enriched by approximately 37‰ and 15‰ in the LPS than the overlying HPS associated with substantial reductions of the NO_3^- and SO_4^{2-} concentration, indicating the occurrence of strong bio-reductions in nitrate and sulfate. The microbial community diversity analyses showed a higher diversity of the denitrifiers encoding *nirS*- (Shannon Index $SI = 6.3$) and *nrf*-type gene ($SI = 2.7$), and the sulfate reduction bacteria (SRB) encoding the *dsr* gene ($SI = 6.4$) in the LPS than in the HPS. The bacterial community structure was influenced by the groundwater hydrochemistry and the redox conditions. Due to the presence of anoxic groundwater with low levels of nutrients, the LPS featured higher abundances of nitrate reducers belonging to *Alphaproteobacteria* and SRB belonging to the strictly anaerobic class *Clostridia* relative to the HPS. Notably, chemolithotrophs were abundant in the LPS and likely coupled the reduction of nitrate with the oxidation of iron. Furthermore, the LPS was demonstrated to attenuate nitrate at a rate two times of the HPS in flow-through experiments, and denitrification accounted for approximately 93% of the nitrate reduction. The high nitrate reduction rate of the LPS was likely attributable to its high functional genes diversity.

* Corresponding author.
E-mail address: lgxu@niglas.ac.cn (L. Xu).

https://doi.org/10.1016/j.scitotenv.2017.11.039
0048-9697/

This study confirmed the occurrence of strong nitrate attenuation in the LPS. The LPS was found to play a significant role in protecting aquifers from anthropogenic contamination.

1. Introduction

The elevated concentration levels of nitrate in groundwater pose significant threats to aquifers from which drinking water is extracted (Rivett et al., 2008). The fate of NO_3^- in low-permeability sediment (LPS), typically consisting of silty and clayey deposits, is of particular interest because aquifers are assumed to be protected from anthropogenic contamination by overlying LPS (Robertson et al., 1996; White et al., 2008). The attenuation of NO_3^- in groundwater has been widely observed in many aquifers (Green et al., 2008; Kim et al., 2009; Nolan and Hitt, 2006; Schaider et al., 2014; Zhang et al., 2009) and in LPS (Dragon, 2013; Feast et al., 1998; Rodvang and Simpkins, 2001), particularly at the boundary between the aquifer and LPS (Hendry et al., 1984; Hill et al., 2000; McMahon, 2001).

In fact, the LPS (e.g., clayey sediments) adjacent to (underlying/overlying) high-permeability zone (HPS, e.g., sand deposit) has also been revealed to be a hot spot of degradation of other contaminants as well, e.g., chlorinated hydrocarbons (Scheutz et al., 2010; Wanner et al., 2016). The attenuation potential of the LPS is thought to be restricted by the small pore sizes of clayey sediments and limited nutrient availability, which may inhibit microbial growth (Lima and Sleep, 2007). However, the LPS in aquifers is believed to greatly influence the attenuation of contaminants because of the effective occurrence of bioreactions and redox zonation resulting from dissolution of minerals in sediments (Hunkeler et al., 2004; Yan et al., 2016). Hence, the degradation capability of LPS remains debated within the scientific community and merits further study.

Nitrate in groundwater could be reduced through processes of denitrification, dissimilatory nitrate reduction to ammonium (DNRA) and anaerobic ammonium oxidation (ANAMMOX). Denitrification is usually considered the primary nitrate removal mechanism in groundwater (Seitzinger et al., 2006), which could be driven by both organic carbon and inorganic electron donors, such as reduced iron and sulfur (Korom, 1992). And a number of studies demonstrated the contribution of DNRA (An and Gardner, 2002; Burgin and Hamilton, 2007) and ANAMMOX (Smith et al., 2015; Zhu et al., 2015) to nitrate removal. The occurrence of all these transforming pathways requires the attendance of microbial communities. Functional genes analysis has been increasingly applied in the study of contaminant attenuation in groundwater (Einsiedl et al., 2015; Herrmann et al., 2015, 2017; Kim et al., 2015). Microbial activity has been recognized to play a significant role in shaping groundwater geochemistry (Akob and Kuesel, 2011; Flynn et al., 2014), which in turn, influences the microbial biodiversity patterns in groundwater. The characterization of groundwater microbial community diversity based on functional genes provides new insights into the relationship between the groundwater environment and the microbial metabolism (Herrmann et al., 2017). Changes in the community structure and the relative abundance of certain species are indicators of the nutrient levels, contaminant concentrations and bio-reduction potential. Hence, the functional genes analysis was used for evaluating the bio-reduction potential and identifying the nitrate removal pathways in the groundwater environment. The *nirS* gene was selected as the functional biomarker for denitrification since it has been demonstrated to be responsible for a key enzyme in the reduction of NO_2^- to NO during denitrification (Braker et al., 1998; Hauck et al., 2001; Herrmann et al., 2017). The presence of microbial communities that have dissimilatory nitrate reduction to ammonium (DNRA) potential was evaluated based on the *nrf* gene (Mohan et al., 2004).

In order to identify the sources of nitrate and occurrence of biodegradation of nitrate and other possible electron acceptor like sulfate in groundwater, stable isotopic analyses were applied in conjunction with the functional genes analysis. The use of multiple isotopes, i.e., ^{15}N and ^{18}O in NO_3^- and ^{34}S and ^{18}O in SO_4^{2-}, although not always conclusive, have been used to successfully discriminate among different sources (Kim et al., 2015; Ma et al., 2016; Stoewer et al., 2015) and to identify relevant bio-reduction processes (Caschetto et al., 2017; Guo et al., 2016; Palau et al., 2010). The stable isotopic fractionation of S and O has also been successfully used to elucidate the biogeochemical pathways of sulfur cycling in various ecosystems (Knoeller et al., 2008; Zhang et al., 2015). For instance, the $\delta^{34}S$ and $\delta^{18}O$ values of the remaining dissolved sulfate have been used to assess the occurrence of dissimilatory sulfate reduction (Choi et al., 2011; Einsiedl et al., 2015). And the *dsr* gene was used to assess the sulfate reduction bacteria (SRB) communities as it has been demonstrated to be a suitable biomarker for SRB (Einsiedl et al., 2015).

The objective of this study was first to examine the occurrence of natural attenuation of nitrate in the LPS and HPS via field investigations in a multi-layer aquifer. Secondly, the bio-reduction potential of the LPS and HPS in attenuating nitrate were evaluated and compared to provide a reference for the agricultural control and groundwater management. To achieve the two goals, the hydrochemical analysis and coupled multi-isotopic method were used to characterize the redox zonation and to identify potential attenuation processes in the LPS and HPS. The microbial composition based on functional genes (*nirS* and *nrf*) targeting nitrate-reducing bacteria was analysed in groundwater from the HPS and LPS to determine the bio-reduction potentials with respect to nitrate. In addition, the *dsr* gene targeting the SRB was analysed to see whether sulfate reduction occurred as well in such groundwater conditions. Finally, laboratory flow-through experiments were conducted with the HPS and LPS to access the overall nitrate reduction rate of the two types of sediment.

2. Material and methods

2.1. Site description and sampling

Groundwater and sediment samples were extracted from the multi-aquifer system at the Tongzhou (TZ) test site near Beijing (Fig. 1a). This site is part of the Integrated Field Research Platform of the Chinese Ministry of Land Resources (MLR). HPS and LPS samples were collected from sediment cores during a hydrogeological field survey. The sediments were sealed and stored in a − 80 °C freezer and thawed at 4 °C before use in the experiments. The HPS and LPS consist of yellowish-brown fine sand and dark-grey silty clay, respectively.

Two multilevel continuous multichannel tubing (CMT) systems (GHTE, Solinst, Canada), referred to as C13 and C33, from the installed CMT matrix were selected for this study (Fig. 1a). Illustrations of the CMT structure and aquifer stratigraphy are shown in Fig. 1b and c, respectively. Sampling campaigns were performed in December 2015 and June 2016 to examine nitrate variations in the two seasons. Groundwater at different levels in the multi-aquifer system was extracted from individual sampling ports (L1, L2, …, L7) of the CMT wells using an inertial pump (Lu et al., 2016). The water was directed into a flow-cell for the measurement of water temperature, pH, electronic conductivity (EC) and dissolved O_2 (DO) in the field using a Multi 350i instrument (WTW, Germany). The redox potential (Eh) was measured with a smart portable probe (BRPSCAN-10, BELL Analytical Instruments Co. Ltd., Dalian, China).

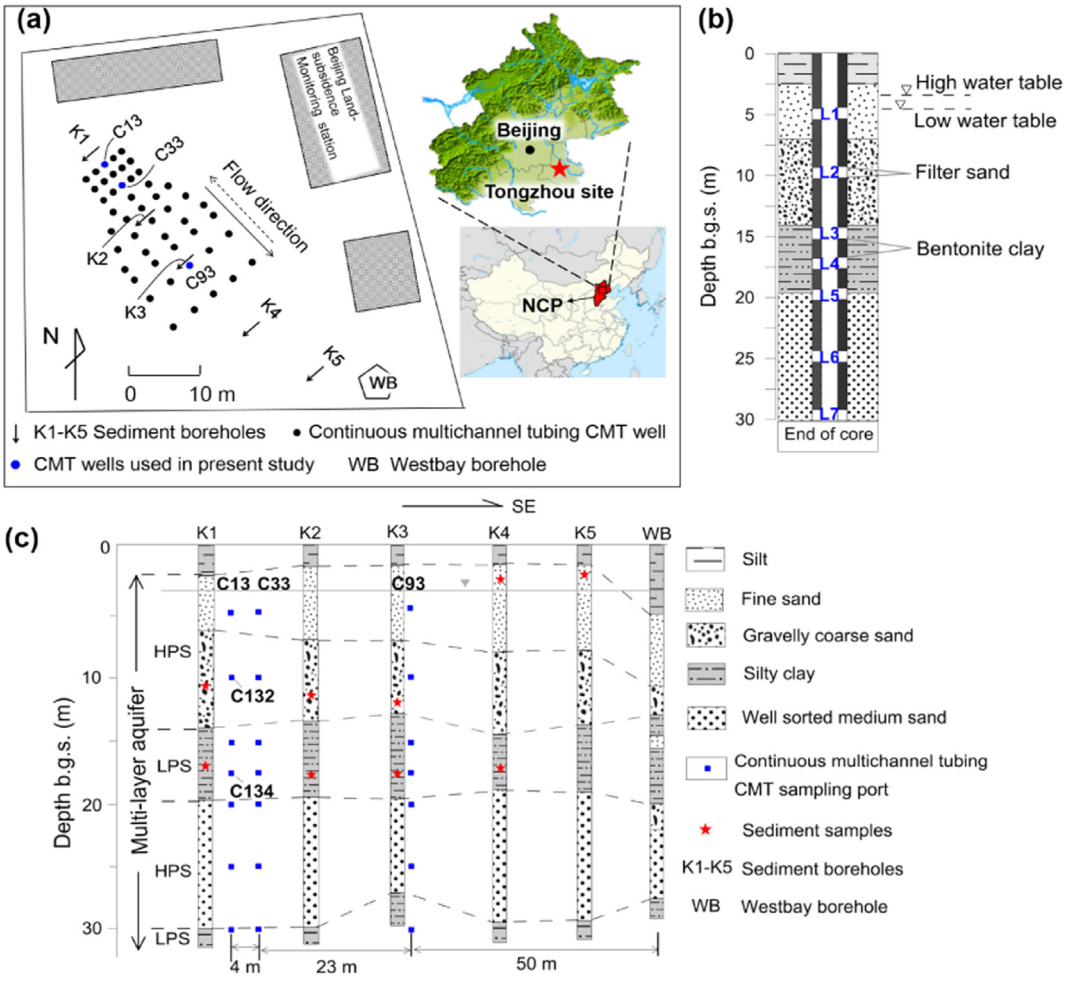

Fig. 1. a) Sketch of the test site and CMT matrix. b) Illustration of the CMT system. c) Geologic logs of the borehole data.

Groundwater samples were filtered through a 0.45 μm membrane filter and stored in acid-washed (20% HCl) polyethylene bottles (for analysing K, Na, Ca, Mg, Mn, As). Samples for cation analysis were acidified to pH < 1 by adding concentrated H_2SO_4. For analysing the Fe(II), 0.2 μm membrane filter was used and samples were measured by colorimetric approach in the field. All samples were preserved at 4 °C in a refrigerator until analysis within two weeks. For the measurement of the $\delta^{15}N$ and $\delta^{18}O$ values of NO_3^-, samples were directly frozen after filtration without acidification. Selected groundwater samples as well as one sediment sample were analysed on the $\delta^{15}N$-NH_4^+ to identify the source of nitrate in groundwater. For the measurement of the $\delta^{15}N$ values of NH_4^+, the filtered and acidified samples were frozen until analysis. In addition, the SO_4^{2-} in groundwater was analysed on their isotope composition to determine whether sulfate reduction occurred as well in such groundwater conditions. For the measurement of the $\delta^{34}S$ and $\delta^{18}O$ values of SO_4^{2-}, filtered (0.45 μm membrane filter) groundwater samples (approximately 2 to 4 l) were acidified to pH < 2 with distilled 6 M HCl, and the SO_4^{2-} in the acidified samples was precipitated as $BaSO_4$ via the addition of a 10% $BaCl_2$ solution.

In addition, groundwater from sampling ports L2 (10 m below ground surface, mbgs) in the HPS and L4 (17.5 mbgs) in the LPS in C13 was extracted to analyse the microbial functional gene composition. Microbial biomass was collected on 0.2 μm cellulose acetate membranes after filtering approximately 3–4 l of groundwater on site, and the filters were stored in dry ice and immediately moved to the laboratory and stored in a − 80 °C refrigerator until DNA extraction and sequencing.

2.2. Sediment analysis and groundwater hydrochemistry and isotope analysis

The grain size distribution of the HPS and LPS was analysed according to the standard methods (NY/T, www.caqs.gov.cn) of the Pipette Method of the Ministry of Agriculture, PRC (NY/T 1121.20-2008). The chemical composition of the sediments was analysed using a wavelength-dispersive X-ray fluorescence (XRF) spectrometer (Model: PW2404, WD-XRF, Philips Inc. Netherlands) after the samples were air-dried. Loss on ignition (LOI) was evaluated by overnight heating at 950 °C (LOI950). The NH_4^+ content was measured via extraction from the sediment with 2 M KCL solution prior to distillation. The total nitrogen content was determined via the Semi-micro Kjeldahl method (NY/T 53-1987). To determine the available-N, including the inorganic nitrogen and hydrolysable organic nitrogen, the Alkali-hydrolysable nitrogen was determined by hydrolysing the sediments with 1.8 mol/l NaOH to convert the hydrolysable nitrogen to ammonium nitrogen, followed by absorption by boric acid which was then quantified by titration with 0.01 mol/l HCl (LY/T1229-1999).

The organic matter content was determined by oxidizing the sediment with a solution of 0.4 mol/l $K_2Cr_2O_7$ and 0.1 mol/l H_2SO_4 (NY/T 1121.6). The cation exchange capacity (CEC) was measured via the titration method with ammonium acetate (NY/T295-1995). In addition, the mineral composition of LPS was determined via X-ray powder diffraction analyses on a 12 kW high-power powder diffractometer (Dmax-MSAL, Rigaku, Japan).

Hydrochemical analysis was performed at the Environmental Laboratory of Peking University. Both major cations (Na^+, K^+, Ca^{2+} and

Mg^{2+}) and major anions (Cl^-, NO_3^- and SO_4^{2-}) were analysed with ion chromatography (but with different instruments: Dionex SOE-033, ICS-1000 and Dionex SOE-033, ICS-2000, respectively). The heavy metals Mn and As were measured via inductively coupled plasma atomic emission spectroscopy (ICP-AES, Perkin-Elmer Optima 3000XL). NH_4^+, NO_2^-, and NO_3^- were analysed with a Continuous Flow Analyzer (CFA; SAN, Skalar Analytical B.V., Netherlands). Blanks and standards were measured routinely to ensure the reliability of the measured hydrochemical data. Fe(II) was measured via the colorimetric method with the reagent 1,10-phenanthroline (HACH Method 8146) as the chromogenic reagent using a DR3900 in the field. The sulfide content was measured via the Methylene Blue Method (HACH Method 10254) using a DR3900 in the field immediately after sampling.

The stable isotopic values of $\delta^{15}N$ and $\delta^{18}O$ in NO_3^- and $\delta^{15}N$ in NH_4^+ were analysed at the Key Laboratory of Dryland Agriculture, Chinese Academy of Agricultural Sciences (Beijing, China) using the denitrifier method (Casciotti et al., 2002; Xu et al., 2013). *P. auerofacins* (ACT 13985) was used as the denitrifier to produce N_2O gas from NO_3^-. The isotopic ratios of $^{15}N/^{14}N$ and $^{18}O/^{16}O$ in the N_2O gas were measured in an isotope ratio mass spectrometer (IRMS, Finnigan MAT Precon-Delta Plus) with a precision of 0.4‰ for $\delta^{15}N$-NO_3^- and 0.3‰ for $\delta^{18}O$-NO_3^-. The internal reference materials USGS32, USGS34 and USGS35 were used to calibrate the $\delta^{15}N$ and $\delta^{18}O$ values, with analytical precisions of 0.05‰ and 0.09‰, respectively. The $\delta^{15}N$ values of NH_4^+ were determined by fixing the ammonium as $(NH_4)_2SO_4$ (Knoller and Strauch, 1999) then combusting and measuring the products in a coupled Elemental Analyzer (EA 3000) and Continuous Flow IRMS (CF-IRMS, IsoPrime 100, Elementar, Germany) with a precision of 0.4‰.

The analyses of $\delta^{34}S$-SO_4^{2-} and $\delta^{18}O$-SO_4^{2-} were completed at the State Key Laboratory of Environmental Geochemistry, Chinese Academy of Sciences (Guiyang, China). In brief, the analyses of the $^{34}S/^{32}S$ and $^{18}O/^{16}O$ ratios in SO_4^{2-} were conducted on the gases SO_2 and CO, respectively, via the combustion of $BaSO_4$ samples at 1030 °C and 1280 °C in EA (EA 3000), followed by measuring the ratio of $^{34}S/^{32}S$ and $^{18}O/^{16}O$ in a CF-IRMS (IsoPrime 100). The international sulfur standards NBS 127 and IAEA were measured twice at three points during each batch of sample measurements as internal standards to ensure a precisions of $<\pm 0.2$‰ for $^{34}S/^{32}S$ and ± 0.5‰ for $^{18}O/^{16}O$.

The stable isotope data ($^{15}N/^{14}N$, $^{18}O/^{16}O$, and $^{34}S/^{32}S$) of the measured samples are reported in the δ notation (in units of ‰) relative to an international standard, as follows:

$$sample(‰) = \frac{R_{sample} - R_{standard}}{R_{standard}} \times 1000 \quad (1)$$

where R represents the abundance ratio of $^{15}N/^{14}N$, $^{18}O/^{16}O$ or $^{34}S/^{32}S$ in the sample and in the standard, respectively. The $\delta^{15}N$ and $\delta^{18}O$ values are expressed relative to Air-N2 (N2 in atmospheric air) and Vienna Standard Mean Ocean Water (V-SMOW), respectively, and the $\delta^{34}S$ values are expressed relative to the Vienna Canyon Diablo Troilite (V-CDT). According to Eq. (1), negative δ values indicate depletion of the heavier isotope, whereas positive δ values indicate enrichment, with respect to the standard.

2.3. Microbiological analysis

To identify the pathways of nitrate removal, three functional gene markers, *nirS*, *nrf*, and *dsr*, were measured. The collected particulates on the filtering membranes (0.22 μm) were stored in a − 80 °C refrigerator until DNA extraction and functional gene analysis. The samples were thawed (4 °C) and centrifuged (12,000*g*) for DNA extraction and PCR amplification. The DNA was extracted using the Powersoil DNA isolation kit (Mobio, USA) according to the manufacturer's instructions. The DNA concentration was determined using a Qubit Fluorometer (Thermo Fisher Scientific). Polymerase Chain Reaction (PCR) techniques were performed on 50 μl mixtures containing 30 ng of DNA, 10 μM of each primer (2 μl), 2.5 mM of each dNTP (4 μl), 10 × *Pyrobest* Buffer (5 μl), 0.3 μl of *Pyrobest* DNA Polymerase (2.5 U/μl, TaKaRa Code: DR005A), and double distilled H_2O (36.7-X). The primer sets (forward and reverse primers) and sequences used for amplification are as follows: *nirS* – Cd3aF/R3cd (AACGYSAAGGARACSGG/GASTTCG GRTGSGTCTTSAYGAA), *nrf* – nrfAF/nrfAR (GCNTGYTGGWSNTGYAA/ TWNGGCATRTGRCARTC), and *dsr* – DSRp2060F/DSR4R (CAACATCGT TCAYACCCAGGG/GTGTAGCAGTTACCGCA). The PCR amplification conditions included an initial step of 95 °C for 5 min; 25 cycles of 30 s at 95 °C, 30 s at 56 °C, and 40 s at 72 °C; and an extension step of 10 min at 72 °C and ending at 4 °C. The quality of the extracted DNA was verified by electrophoresis on 2% agarose gels (150 V; 30 min). The purified PCR products obtained from *nirS* and *nrf* and *dsr* gene amplifications from each triplicate treatment were blended in equal amounts and then sequenced using Illumina MiSeq paired-end protocol performed by ALLWEGENE Technology Co., Ltd. (Beijing, China). Clean tags were grouped into operational taxonomic units (OTUs) at 97% similarity. A representative sequence for each OTU was selected by BLAST search, and its identity was classified using the RDP classifier. The sequence data were analysed using the software QIIME (v1.8.0) to construct a systematic tree and to generate the community diversity indices (Chao1 estimator and Shannon index).

2.4. Flow-through experiments

Flow-through experiments were performed to evaluate the overall nitrate reduction rate of the LPS and HPS using stainless steel columns with an internal diameter of 3.5 cm and a length of 20 cm. The bottoms and tops of the columns were equipped with two chambers consisting of 1.5 cm of evenly packed quartz sand and a mesh with a membrane (0.22 μm) to create uniform flow. To avoid side flow, the inner column wall was coated with Vaseline. The columns were carefully wet packed with dry-sieved sediment materials (grain size: <1 mm) in 10 increments following the "wet-packing" approach of Li et al. (2014). A phosphate buffered solution (pH = 7) of Br^- and NO_3^- (prepared with 100 mg/l KBr and KNO_3) was pumped into the bottom of the column by a high-performance liquid chromatography (HPLC) pump (LabAlliance Series III Pump, flow accuracy: 1%, flow precision: 0.2% RSD) at a constant flow rate of 0.1 ml/min. Prior to each experiment, the columns were pre-conditioned for 4 days until the NO_3^-, NO_2^- and NH_4^+ in the effluent were below the detection limit. The effluent was sampled every 1 h by an automatic sampler to measure the concentrations of the conservative tracer Br^-, as well as the concentrations of NO_3^-, NO_2^-, and NH_4^+ as indicators of the nitrate reduction pathways. Br^- was measured with a selective ion electrode (MP 523-06, SanXin Co. Ltd., Shanghai; accuracy: ±2.5%). The concentrations of NO_3^-, NO_2^- and NH_4^+ were determined with the CFA (SAN, Skalar Analytical B.V., Netherlands).

3. Results

3.1. Physicochemical composition of the sediment

The LPS and HPS are classified as silty clay and medium sand according to their grain size distributions (Table 1). The sediment pH value of the LPS was lower than the HPS. The LPS had higher contents of organic matter (7.03 g/kg), TN (0.073%), alkali-hydrolysable N (A-N) (57.5 mg/kg) and CEC (281 mmol/kg(+)) than the HPS. Regarding to the inorganic N, the LPS contained slightly lower amount of NH_4^+-N than HPS, but high amounts of NO_3^--N (104.6 mg/kg) and NO_2^--N (54.2 mg/kg). Mineralogically, the LPS is composed of 41% quartz (SiO_2), 19% albite ($(Na,Ca)Al(Si,Al)_3O_8$), 16% calcite ($CaCO_3$), 9% clinochlore ($(Mg,Al,Fe)_6(Si,Al)_4O_{10}(OH)_8$), 5% dolomite ($CaMg(CO_3)_2$), 4% mica ($KAl_2Si_3AlO_{10}(OH)_2$), 4% K-feldspar ($KAlSi_3O_8$), and 2% pyrite ($FeS_2$). The major chemical constituents (oxides) of the LPS and HPS are shown in Table 2. CaO and MgO are more abundant in the LPS

Table 1
Sediment characteristics.

Parameter		Unit	LPS (%)	HPS (%)
Grain size	250–2000	μm	0.71	67.2
	50–250		11.89	31.98
	10–50		62.63	1.73
	5–10		11.83	0.15
	1–5		7.76	1.1
	<1		5.18	2.32
pH			7.68	8.44
NH_4^+-N		mg/kg	45.7	50.9
NO_3^--N		mg/kg	104.6	N.A.
NO_2^--N		mg/kg	54.2	25.3
Alkali-hydrolysable nitrogen		mg/kg	57.7	7.19
Total nitrogen (TN)		%	0.073	0.024
Organic matter		g/kg	7.03	2.30
Cation exchange capacity (CEC)		mmol/kg(+)	281	57.2

than in the HPS. Fe-oxides (Fe_2O_3 + FeO) represent 9.66% and 2.83% of the LPS and HPS, respectively. The Fe-accompanying element Mn (−oxide) was correspondingly high in the LPS (~3.8 times that in the HPS).

3.2. Hydrochemical profiles

The vertical profiles of hydrochemical parameters analysed in groundwater from the two CMT systems (C13 and C33) are shown in Fig. 2. The detailed values of all the measured parameters in June 2016 were listed in Table S1 and S2. The dissolved O_2 (DO) changed from 0.3–0.6 mg/l near the groundwater table at 5 mbgs to <0.15 mg/l at 10–30 mbgs (Fig. 2b). The oxidation-reduction potential (ORP) values reported as Eh were negative at each port, ranging from −300 to −600 mV. The vertical profiles of K, Na and Ca were similar and showed similar decreasing trends from 5 mbgs to 30 mbgs. The Mg concentrations tended to increase with depth. The concentrations of the dissolved heavy metals Mn, and As as well as NH_4^+ showed similar vertical profiles with distinct higher concentrations detected in the LPS than in the neighbouring HPS aquifers. Notably, the Fe(II) concentrations were particularly high at 10 mbgs in the HPS. The values of Fe(II) measured in other sampling campaigns were listed in Table S3.

The concentrations of NO_3^-, SO_4^{2-} and Cl^- were higher in the HPS than in the LPS. Both the NO_3^- and SO_4^{2-} concentrations decreased with depth from the HPS to the lower limit of the LPS. And the NO_3^- was not detectable below the lower limit of the LPS. Notably, the NO_3^-, NO_2^-, NH_4^+, SO_4^{2-}, and HS^- concentrations in the groundwater showed an abrupt change from 10 mbgs in the HPS to 15 mbgs near the boundary between the HPS and the LPS.

3.3. Isotopic compositions of NO_3^- and SO_4^{2-}

In the winter sampling campaign, the nitrate concentrations were all lower than 2 mg/l in both CMTs and showed the decreasing trend with depth, with no detectable nitrate (<0.1 mg/l) at ports L6 and L7 (SI Table S4). To identify the source of nitrate in the groundwater, the values of $\delta^{18}O\text{-}NO_3^-$ versus $\delta^{15}N\text{-}NO_3^-$ were plotted in Fig. 3, and the characteristic isotopic ranges for different sources were taken from Kendall (1998) and Xue et al. (2009). The winter data points (marked with blue symbols in Fig. 3) are clearly distributed in two areas, which are outlined with dashed lines. The values of $\delta^{15}N\text{-}NO_3^-$ in groundwater from port L1 (5 mbgs, marked with blue and red triangles) from the two CMTs ranged from +10‰ to +18‰. In the groundwater from ports L2 to L5 in winter, the $\delta^{15}N$ values ranged from −0.3‰ to +4.3‰, and the $\delta^{18}O$ values ranged from +30‰ to +65‰.

In contrast, the vertical distributions of NO_3^- isotopic compositions and concentrations in summer showed quite different patterns from those in winter. In early summer (June 2016), the nitrate concentrations increased dramatically to 0.9–30 mg/l in the HPS and were detectable but at very low levels in the LPS (Tables S1, S2). The $\delta^{15}N$ and $\delta^{18}O$ values of NO_3^- in groundwater at port L1 did not change much between the two seasons. However, the isotopic composition of the nitrate in the groundwater below L2 changed markedly. The $\delta^{15}N$ values in the groundwater from L2 increased from +0.6–+1‰ in winter (December 2015) to +8–+16‰ in summer (June 2016). Notably, the values of both $\delta^{15}N\text{-}NO_3^-$ (−20‰–−22‰) and $\delta^{18}O\text{-}NO_3^-$ (+5.6–+7.5‰) were very low in the groundwater from port L3 (15 mbgs) near the boundary between the HPS and the LPS. In addition, the vertical profiles of the nitrate concentrations and the $\delta^{15}N\text{-}NO_3^-$ and $\delta^{18}O\text{-}NO_3^-$ values in June 2016 are shown in Fig. 4a.

The vertical profiles of SO_4^{2-} concentrations and the $\delta^{34}S\text{-}SO_4^{2-}$ and $\delta^{18}O\text{-}SO_4^{2-}$ values are shown in Fig. 4b. The concentration of SO_4^{2-} decreased dramatically with depth from L1 to L3 near the upper limit of the LPS. The vertical profiles of the $\delta^{34}S\text{-}SO_4^{2-}$ and $\delta^{18}O\text{-}SO_4^{2-}$ values showed similar trends with depth throughout the whole multi-layer aquifer system from L1 to L7. The values of $\delta^{34}S\text{-}SO_4^{2-}$ and $\delta^{18}O\text{-}SO_4^{2-}$ were more enriched by 17.5‰ and 7.9‰, respectively, in the LPS than in the HPS.

3.4. Phylogenetic analyses of *nirS*, *nrf* and *dsr* genes in groundwater from the HPS and LPS

The *nirS*, *dsr* and *nrf* OTUs were identified to the most closely related representatives by BLAST search with similarities of 78–100%. The values of fractions and identities of the most abundant OTUs were listed in Table S5, S6, S7. The relative abundance of phylogenetic classes for *nirS*, *nrf* and *dsr* in the LPS and HPS are shown in Fig. 5. *Proteobacteria* was the dominant phyla of *nirS*-type denitrifiers in the identified sequences at both depths. The most abundant *nirS*-type denitrifiers in the LPS were related to *Betaproteobacteria* (49.4%), and the relative abundance of *Gammaproteobacteria* decreased to 15.6%. In contrast, the HPS was characterized by high relative abundances of *Gammaproteobacteria* (57.7%) and *Betaproteobacteria* (39.1%) *nirS*-type denitrifiers. Notably, the *nirS* community members in the LPS exhibited a much higher fraction of *Alphaproteobacteria* (6.3%) than the overlying HPS (0.96%).

The most abundant *nirS*- and *nrf*- denitrifiers and *dsr*- SRB identified with high similarities (> 95%) at the species level in the two samples are plotted in Fig. 6. The *nirS* denitrifiers in the LPS consisted of diverse species related to *Sulfuritalea hydrogenivorans* (8%), *Sulfuricella denitrificans* (5.7%), *Dechloromonas* (5.7%), *Azoarcus* (4.7%), *Vogesella* (4.6%), *Dechlorospirillum* (3.8%) and *Rhodanobacter* (3.4%). Other abundant *nirS* species in the LPS were *Thiobacillus denitrificans*, *Leptothrix cholodnii* and *Ideonella*. In addition, a fraction of 5.9% *nirS* sequences in the LPS were identified closely related to *Pseudomonas stutzeri* with a medium similarity (91%). And a total of approximately 30% *nirS* sequences in the LPS remained unidentified. In the groundwater from HPS, a fewer number of species constituted the *nirS* denitrifiers compared to the LPS. *Pseudomonas stutzeri* (56.3%) with a 100% similarity constituted the majority of the *nirS* denitrifiers (Fig. 6a). And 10% of the *nirS* denitrifers in the HPS were closely related to *Thiobacillus denitrificans* at a similarity of 92%. The *Sulfuritalea hydrogenivorans* and

Table 2
Major elements in the sediment.

Inorganic compound (%)	LPS	HPS
SiO_2	51.37	72.87
Al_2O_3	14.05	13.10
Fe_2O_3	5.93	2.19
MgO	2.87	0.953
CaO	7.57	1.97
Na_2O	1.30	3.60
K_2O	2.71	3.46
MnO	0.126	0.033
TiO_2	0.692	0.320
P_2O_5	0.161	0.087
FeO	1.73	0.64

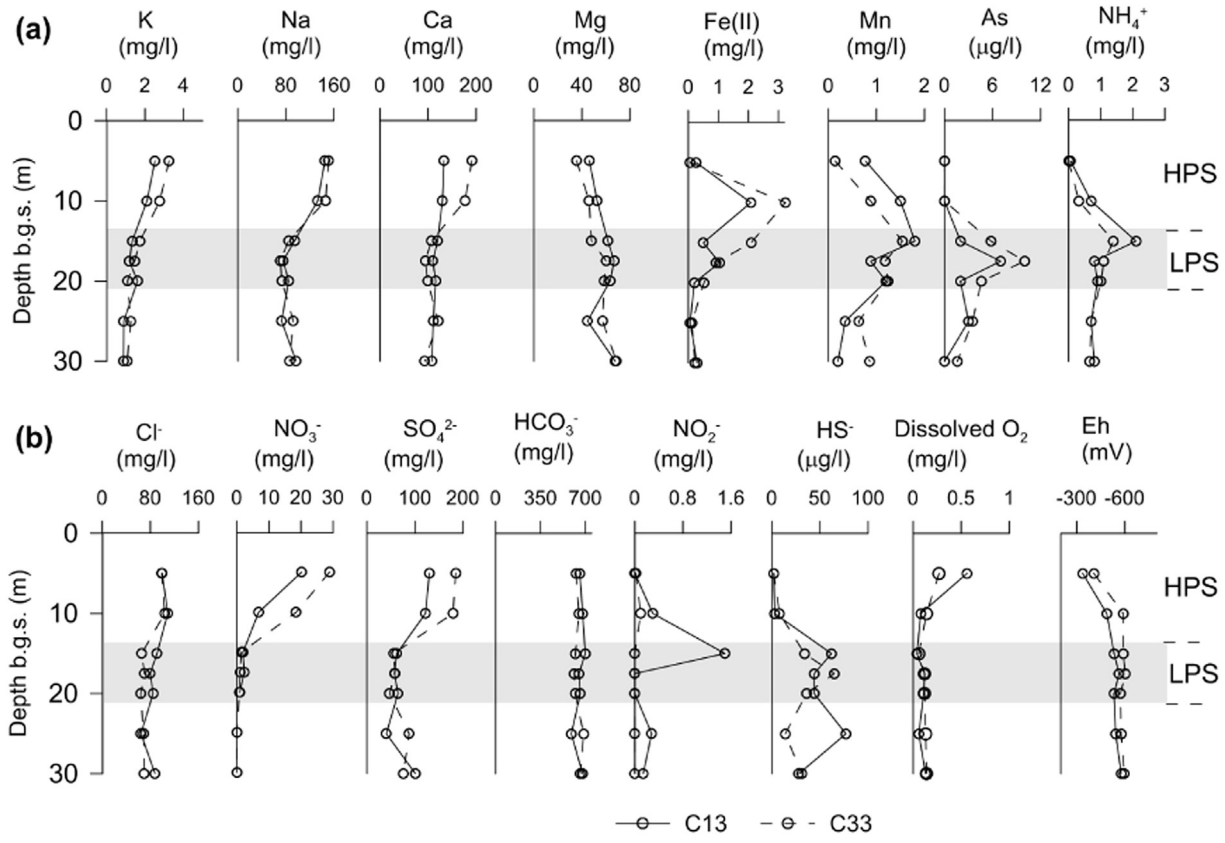

Fig. 2. a) Profiles of cations in groundwater of the selected CMT wells (C13 and C33) in the test site measured in June 2016. b) Profiles of the main anions and dissolved O_2 and redox potential in the selected CMT wells.

Sideroxydans lithotrophicus comprised 5% and 3.5% of the *nirS* denitrifiers in the HPS. The *Sideroxydans lithotrophicus* was however, nearly absent in the LPS.

In terms of DNRA, the *nrf*-type communities in the LPS belonged to *Alphaproteobacteria* (44.3%), which were absent in the HPS. *Gammaproteobacteria* (27.8%) appeared only in the HPS. In addition,

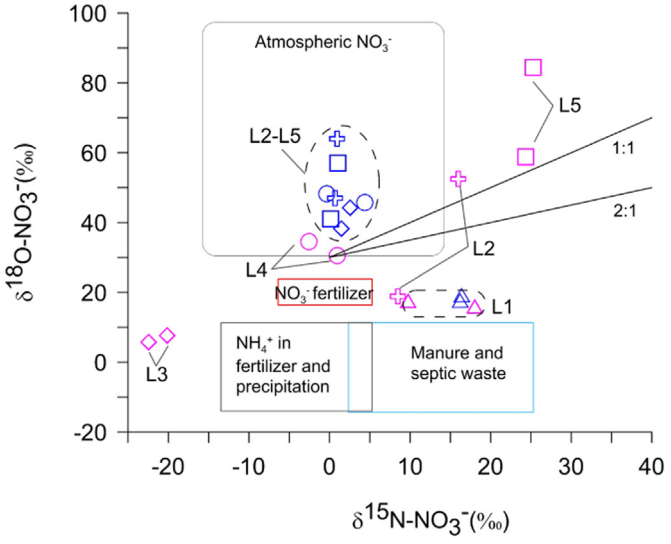

Fig. 3. $\delta^{18}O$ versus $\delta^{15}N$ values for nitrate in groundwater at each level (L1, L2, …, L5) of the CMT monitoring wells C13 and C33 during the two sampling campaigns (Blue and purple-red symbols denote to data points measured in December 2015 and June 2016). The ranges of $\delta^{18}O$ and $\delta^{15}N$ compositions for different nitrate sources were taken from Kendall (1998) and Xue et al. (2009).

large portions of the *nrf*-type communities in the groundwater from both the LPS and HPS belonged to the class *Bacilli* of phylum *Firmicutes*, whereas members of this phylum were not present in the *nirS*-type denitrifier communities. The majority of *nrf* members in the LPS were closely related to the species *Candidatus Puniceispirillum marinum* (44%), a member of *Alphaproteobacteria*, and *Bacillus thuringiensis* (35%) (Fig. 6c). Additionally, *E. coli* (27.8%) was the dominant *nrf* denitrifier in the identified sequences of the HPS. And the *nrf* denitrifiers belonging to the species *Clostridum tetani* (8%) were present only in the LPS.

The *dsr*-type SRB communities in the groundwater from both the LPS and HPS were clearly dominated by phyla related to *Deltaproteobacteria*, and members of this class accounted for a slightly higher fraction of the communities in the HPS than in the LPS (Fig. 5). However, the proportion of *dsr*-type SRB belonging to the class *Clostridia* was two times of that in the groundwater of the LPS than in that of the HPS. The most abundant *dsr*- SRB were related to the species *Desulfobulbus propionicus* at a relative abundance of 20.4% and 17.7% respectively, in the LPS and HPS (Fig. 6b). Other *dsr*- SRB of high relative abundances in the LPS were *Desulfotomaculum putei* (8.8%), *Desulfobacca acetoxidans* (8.4%), *Desulfatiglans anilini* (6.8%). The less abundant genera *Desulfurivibrio* (3.1%), *Desulfobacula toluolica* (2.7%), *Desulfovirga adipica*, *Desulfatiferula* and *Syntrophobacter fumaroxidans* in the LPS were almost absent in the HPS. In contrast, the *dsr*- SRB in the groundwater from the HPS also featured the species *Desulfofaba fastidiosa* (15.6%), *Desulfococcus oleovorans* (5.6%) *Thermodesulforhabdus norvegica* (3.9%) and *Desulfacinum infernum* (3%), which were exclusively present in the HPS.

3.5. Breakthrough curves from the flow-through experiments

The microbiological diversity analyses of the *nirS* and *nrf* genes in groundwater from the field site demonstrated higher diversities of

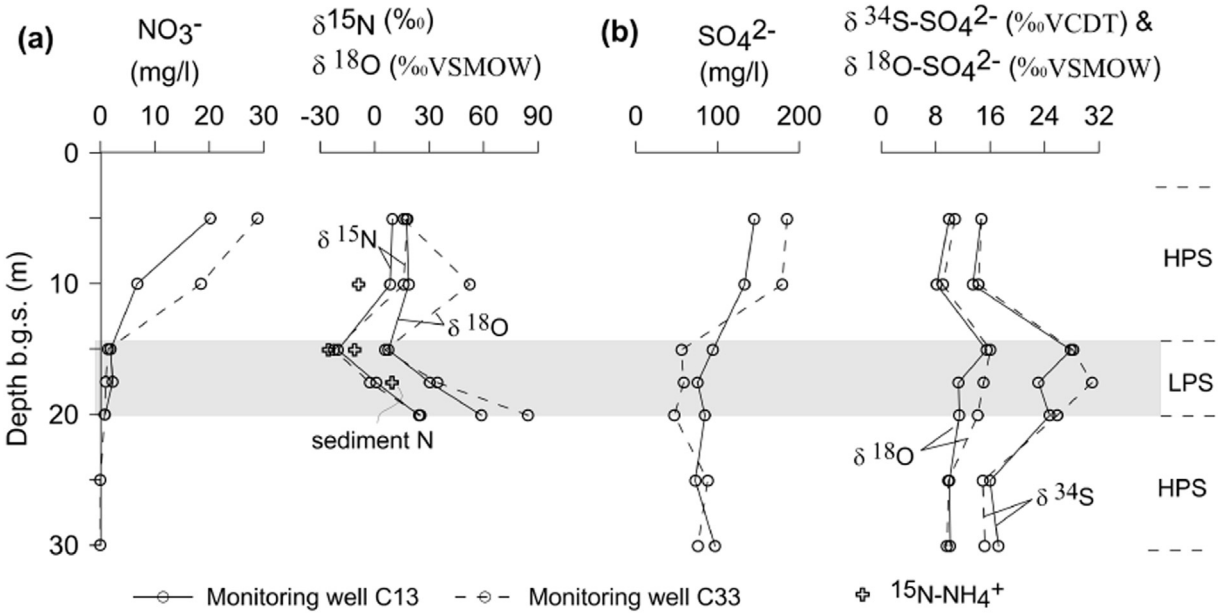

Fig. 4. Vertical profiles of concentration, $\delta^{15}N$ and $\delta^{18}O$ values in NO_3^- and $\delta^{15}N$ values NH_4^+, $\delta^{34}S$ and $\delta^{18}O$ values in SO_4^{2-} in the two CMT monitoring wells C13 (solid lines) and C33 (dashed lines).

microbes that capable of denitrification and DNRA in the LPS than in the HPS. In the laboratory, the overall nitrate reduction potential of the two sediment types was assessed via flow-through experiments. The breakthrough curves (BTCs) of non-reactive tracer Br^- (as a reference) and the reactive solute NO_3^- in the effluent of the two columns are shown in Fig. 7a. The concentrations of Br^- and NO_3^- were normalized by dividing by the initial concentrations in the inflow. The normalized peak concentration of Br^- in the effluent was 1 for both sediments, whereas the normalized peak concentration of NO_3^- was 0.55 and 0.79 for the LPS and the HPS, respectively. The nitrate reduction products NO_2^- and NH_4^+ were also monitored in the effluent to identify the nitrate reduction pathways. Fig. 7b and c show the BTCs of NO_2^- and NH_4^+ in the effluent of the LPS column. The increases in NO_2^- and NH_4^+ were synchronous with the decrease in nitrate.

4. Discussion

4.1. Sediment composition and groundwater hydrochemistry

The analysis of sediment composition showed high TN, A-N, NO_3^--N and NO_2^--N in the LPS, indicating the entrapment of N-bearing ions in history (Table 1). Higher CEC in the LPS than the HPS indicated that metal cations are likely to be adsorbed to the clay minerals in LPS sediments. The groundwater was hypoxic to anoxic in the HPS, while anoxic conditions prevailed in the LPS. The ORP was very low throughout the multi-layer aquifer indicating that the groundwater was under strongly reducing conditions.

The vertical distributions of K, Na and Mg in groundwater were in agreement with those of the corresponding oxides K_2O, Na_2O and MgO within the associated sediments. However, the concentrations of

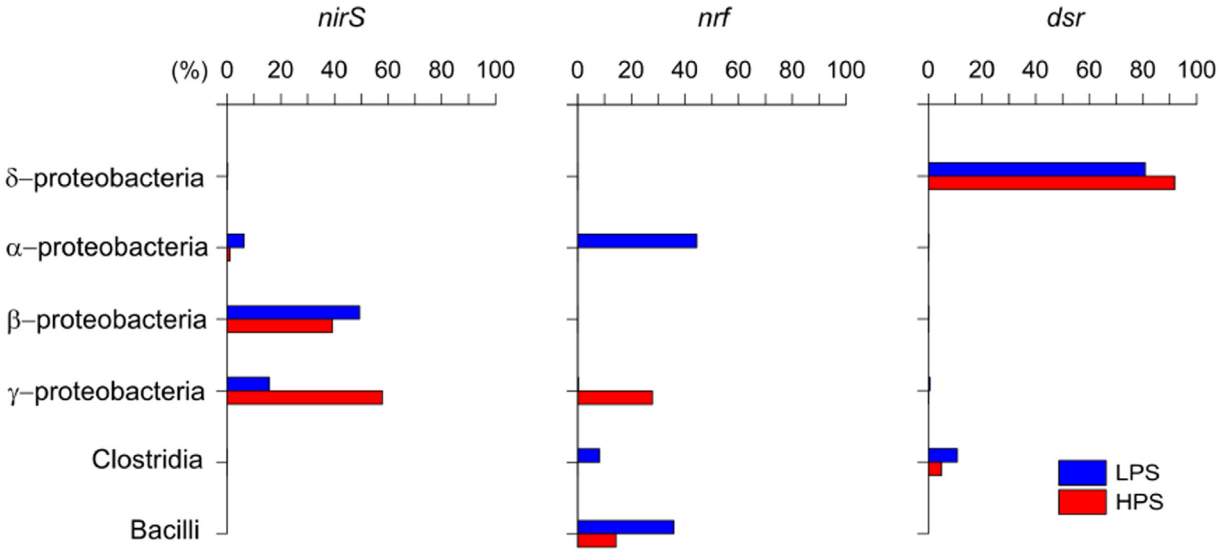

Fig. 5. Bar plot of relative abundance of phylogenetic classes for NirS, SRB and DNRA in LPS and HPS.

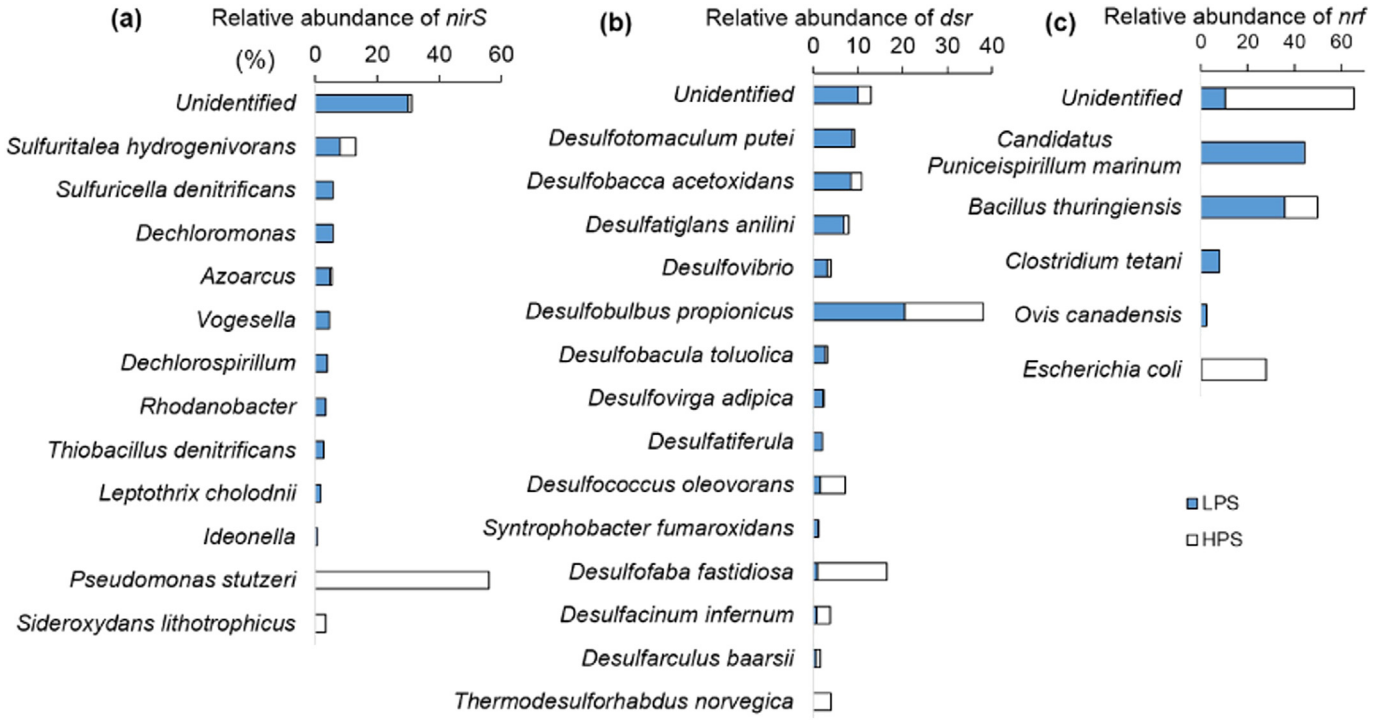

Fig. 6. Relative abundance of *nirS*, *nrf*-denitrifers and *dsr*-SRB at the genus and species level in LPS and HPS.

Ca in groundwater (Fig. 2a) appeared to be higher in the overlying HPS than LPS although the HPS has a lower content of Ca-oxide CaO than the LPS (Table 2), indicating likely extra inputs of Ca-related fertilizers into the overlying HPS. The ferrous iron Fe(II) showed distinct high concentrations in the groundwater at 10–17.5 mbgs (lower part of HPS and upper part of LPS), and a decreasing trend with depth within the LPS in June 2016. The high dissolved iron contents in the groundwater of HPS and LPS were likely due to the dissolution of solid Fe-oxides and pyrite in the sediments. However, the total dissolved Fe in groundwater showed particular high concentrations at 17.5–20 mbgs in the LPS during previous field samplings in 2014 and 2012 (Table S3). This demonstrated that the redox state of iron in groundwater was prone to change in the two types of sediments. In addition, the dissolved heavy metal contents (Fe, Mn and As) and sulfide HS^- in the groundwater were likely attributed to the reducing conditions (Guo et al., 2008). Sulfide might be produced from the dissimilatory sulfate reduction (DSR) (Druhan et al., 2014) and subsequently precipitates with Fe(II) to FeS and FeS_2 (Noel et al., 2017), leading to the low levels of sulfide concentrations in groundwater. And Fe and Mn elements may act as potential electron donors for chemolithotrophic denitrification in addition to the organic matter (Rivett et al., 2008).

High concentrations of NO_3^-, Cl^-, SO_4^{2-}, K, Na, and Ca in the upper HPS might be attributable to extensively applied inorganic fertilizers in addition to mineralogical dissolution as the test site is nearby the local agricultural farmlands. The abrupt simultaneous increases in NO_2^-, NH_4^+ and HS^- at the boundary between the HPS and LPS were likely attributed to the high reducing condition, and strongly implied the occurrence of biologically mediated reduction of NO_3^- and SO_4^{2-}.

4.2. Bio-reduction of nitrate and sulfate based on coupled isotopic compositions of NO_3^- and SO_4^{2-}

To verify whether the reduction of NO_3^- and SO_4^{2-} was facilitated by microorganisms, the isotopic analyses of N, S, and O were performed. The $\delta^{15}N$ values (Fig. 3 and Table S4) were lower than the values reported for ammonium fertilizer in the literature (Xue et al., 2009). Although the isotopic composition of ammonium fertilizer applied in the region was unknown, the low $\delta^{15}N$ and $\delta^{18}O$ values suggested that NO_3^- was likely sourced from biogeochemical processes, e.g., nitrification of ammonium from fertilizers or DNRA. Organic nitrogen in the sediments was another likely source of NO_3^- in the groundwater. However, the $\delta^{15}N$-NH_4^+ value of solid organic nitrogen was +9.5‰, which was quite different from that of the groundwater, which ranged from −8.8‰ to −25‰. Hence, the nitrate in the groundwater near the boundary between the HPS and the LPS most likely originated from synthesized ammonium fertilizer with low $\delta^{15}N$ values. Furthermore, the data points from L2 to L5 appeared to be linear with a positive slope of 0.86 ($^{15}N/^{18}O$), which was smaller than the 1:1 denitrification line. However, the strong enrichment in ^{15}N and ^{18}O in NO_3^- with depth from L3 to L5 throughout the LPS in association with decreasing nitrate concentration implied the occurrence of nitrate bio-reduction processes.

The isotope composition of nitrate in shallow groundwater (5 mbgs at port L1) in both seasons suggested a likely source from manure and septic waste. However, the $\delta^{18}O$-NO_3^- values in groundwater from L1 were higher than the reference range. This divergence may have been caused by the analytical denitrifier method, which has been demonstrated to result in higher $\delta^{18}O$ values than the silver nitrate method (Kendall et al., 2007). Compared to the reference isotope values, nitrate in groundwater from ports L2 to L5 in winter was likely from atmospheric deposition (Fig. 3). The vertical distribution of $\delta^{15}N$-NO_3^- values and NO_3^- concentrations indicated the absence of agricultural activities during winter. The more enriched $\delta^{15}N$ values in groundwater at port L2 (10 mbgs) in summer than in winter might have been caused by mixing with the overlying groundwater (with high $\delta^{15}N$ values) via vertical downward transport with rainfall. The higher $\delta^{34}S$-SO_4^{2-} and $\delta^{18}O$-SO_4^{2-} values in the LPS than in the HPS aquifers suggested the occurrence of strong sulfate reduction in this zone. Based on the vertical profiles of sulfate concentration and the S and O isotopic compositions, an active sulfate reduction zone was identified at 10–18 mbgs in the aquifer.

4.3. Microbial community diversity in the LPS and HPS

As an overview of the microbial diversity represented by functional genes in the two zones, OTU-based community diversity indices

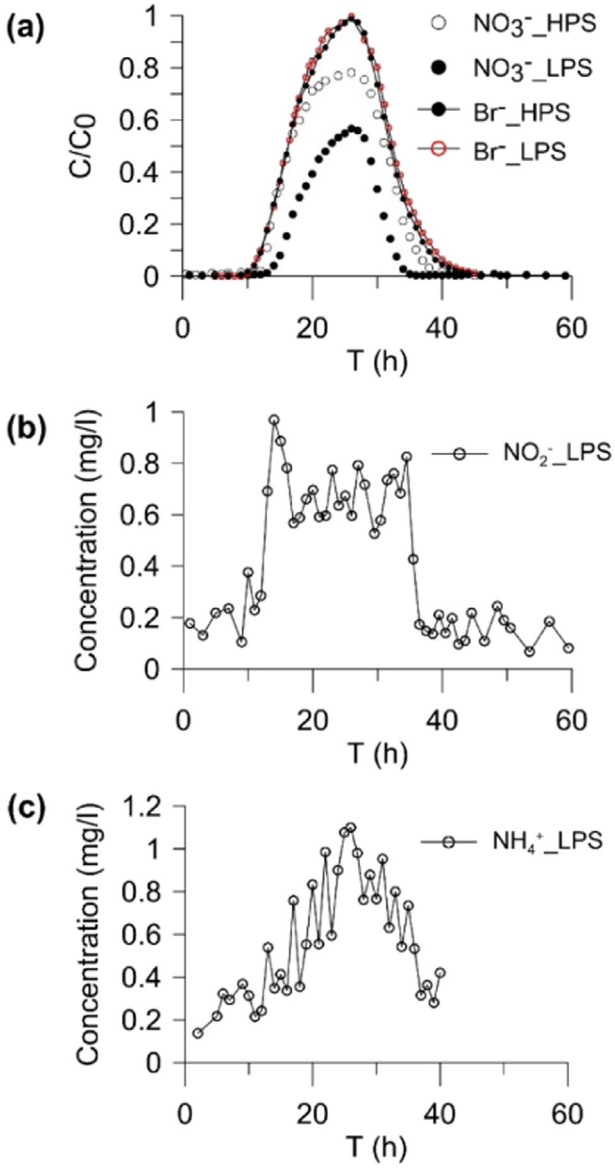

Fig. 7. BTCs of the tracer, the reactant and the products in effluent from columns packed with HPS and LPS in flow-through experiments. (a) BTCs of Br^- and NO_3^- in effluent from both columns; (b) BTC of NO_2^- in effluent from the column packed with LPS; (c) BTC of NH_4^+ in effluent from the column packed with LPS.

(i.e., the Chao1 estimator, Shannon index, SI, and the phylogenetic diversity, PD) were calculated using UPASE in QIIMW and summarized in Table 3. Higher SI and PD values indicated higher diversities in the samples. The observed species and PD values for all genes are higher in the LPS than in the HPS. The SI values are also higher for the *nir*S and SRB communities in the LPS than in the HPS. All the indices demonstrate that the functional gene diversity were higher in the LPS than in the HPS. Based on OTU richness, the *nirS*-type denitrifier communities were more diverse in the LPS than in the HPS.

Table 3
Diversity index results for the LPS and HPS.

			Observed species	Reads	OTUs	Chao1	Shannon index	Phylogenetic diversity (PD)
nirS	HPS	C132	785	52062	785	787	3.6	149
	LPS	C134	1101	66378	1119	1140	6.3	196
SRB	HPS	C132	787	56363	789	799	5.5	85
	LPS	C134	1031	51264	1031	1031	6.4	146
DNRA	HPS	C132	59	71294	59	59	2.2	23
	LPS	C134	149	107146	155	160	2.7	31

The aerobic heterotrophic species *Pseudomonas stutzeri* in groundwater from the LPS were present at a substantially lower relative abundance than in the HPS, highlighting the constraints on the aerobic metabolic lifestyle in the LPS. *P. Stutzeri* could, however, oxidize ferrous iron under anaerobic autotrophic conditions but at a comparatively slower rate than under aerobic conditions (Straub et al., 1996). This ability might be the metabolic pathway of *P. Stutzeri* in the anaerobic LPS, which contains abundant potential iron electron donors. The *nirS* denitrifiers in the LPS were featured by abundant thiosulfate- and hydrogen-oxidizing autotrophic bacterium *Sulfuritalea hydrogenivorans*. While *Thiobacillus denitrificans* and *Sideroxydans lithotrophicus* were the chemolithoautotrophic bacterium of high relative abundance in the HPS, which has the iron-oxidizing potential. Based on OTU richness, the *nirS*-type denitrifier communities showed a higher diversity in the LPS, containing more diverse lithoautotrophs, the hydrogen- and sulfur-oxidizing *Sulfuritalea* and *Sulfuricella* and iron- and manganese-oxidizing *Leptothrix* (1.7%) as well as heterotrophic denitrifiers (*Azoarcus*, *Rubrivivax*, and *Ideonella*) than the HPS.

The presence of the iron-oxidizing *Dechloromonas* and the species *Dechloromonas aromatic* (0.2%) in the LPS, which is commonly found in groundwater contaminated with organic compounds such as benzene, implied potential historical contamination of the groundwater with organic pollutants, which likely became trapped in the LPS. The abundant *Dechlorospirillum* in *Alphaproteobacteria* in the LPS were capable of reducing perchlorate and oxidizing Fe(II). Other *nirS* denitrifiers in the LPS, *Rubrivivax gelatinosus*, *Rhodanobacter* have been demonstrated to be the primary populations that biodegrade organic compounds and influence the redox state of heavy metals in contaminated groundwater (Hemme et al., 2016; Zein et al., 2004). Compared to the HPS, the LPS appeared to feature a higher diversity of *nirS*-type denitrifiers that metabolize heavy metals and organic contaminants in addition to natural organic matter.

The dominant *nrf* denitrifiers *Candidatus Puniceispirillum marinum*, in the class of *Alphaproteobacteria*, in the LPS is a metabolic generalist with versatile functional genes for reducing inorganics, nitrate, sulfate and phosphate, typically in marine environments (Oh et al., 2010). This study is the first to report the presence of abundant *Candidatus Puniceispirillum marinum* in association with DNRA in pristine groundwater. Notably, *E. coli* in the class of *Gammaproteobacteria* was found to be the main *nrf* nitrate reducers in the identified sequences in the HPS. This bacterium can reduce nitrite under anaerobic conditions using the nitrite reductases *NrfA* and *NirB* (Khlebodarova et al., 2016; Kim and Hur, 2017). The presence of *E. coli* in the HPS also indicated potential groundwater contamination by pathogens from sanitary sewage. The high abundance of *Alphaproteobacteria* in the LPS, in contrast to the *Gammaproteobacteria* in the HPS, demonstrated that the *nrf*-type nitrate reducers adapted to the groundwater conditions characterized by low levels of nutrients, organic carbon (OC) and nitrate.

The most dominant *dsr* SRB species was *Desulfobulbus propionicus* in both the two depths of groundwater. In addition to a sulfate reducer, *Desulfobulbus propionicus* was also very active in anaerobic sulfate production coupled to the Fe(III) and Mn(IV) reduction (Lovley and Phillips, 1994). This indicated that the sulfur cycling in groundwater was likely coupled to the redox change of iron and manganese. In addition, the genera *Desulfotomaculum*, *Desulfatiglans anilini* and *Desulfobacula toluolica* were aromatic compound-degrading bacterium, which were capable of reducing phenol and the BTEX (Farhadian et al., 2008; Suzuki et al., 2014). The proportions of the strictly anaerobic *Syntrophaceae*, Clostridia *Desulfotomaculum* and *Desulfobulbus* were higher in the LPS than in the HPS. Notably, these groups are common in hydrocarbon-contaminated aquifers (Kleikemper et al., 2002; Morasch et al., 2004). The diverse SRB populations characterized by the *dsr*-type gene suggested as well groundwater in this test site was likely contaminated by organic compounds.

Overall, the phylogenetic compositions of the microbial communities based on specific functional genes demonstrated that the patterns of community structure shifted with changes in the groundwater environment. The heterotrophic aerobic communities tended to be replaced by the lithotrophic anaerobic communities in the deep LPS. In carbon-limited systems, alternative electron donors other than OC, such as reduced Fe, Mn, S and organic compounds, are likely used for the reduction of nitrate and sulfate. The microbial composition in the LPS showed high potential for the occurrence of chemolithotrophic nitrate reduction coupled to sulfur and iron oxidation. The autotrophic species more adapted to the low-OC conditions played a more significant role in nitrate reduction.

4.4. Nitrate reduction rate in LPS & HPS

Additional batch tests indicated that neither sediment type exhibited nitrate adsorption (Wang, 2014). Therefore, because NO_3^- was not adsorbed by the sediment grains, the reduction in the nitrate concentration in the two columns most likely occurred via the biodegradation of nitrate.

The increases in NO_2^- and NH_4^+ were synchronous with the decrease in nitrate, suggesting that they were likely generated via nitrate transformation. Based on the flux of NO_3^-, NO_2^- and NH_4^+ in the effluent, the mass of nitrate decreased by 56.8% and 28.1% in the LPS and HPS columns, respectively. In the LPS column, the produced NH_4^+ and NO_2^- accounted for 7% and 3% of the nitrate reduction, indicating that NO_2^- was primarily (90%) reduced to final gas products. Hence, the majority (93%) of NO_3^- was reduced through denitrification under the experimental conditions (pH = 7). The NH_4^+ was likely produced through DNRA. The microbial analysis of ANAMMOX bacteria was not successful due to the low DNA concentrations in the samples. Therefore, the appearance of the NO_2^- and NH_4^+ BTCs in the flow-through experiments of the LPS and the results of the *nirS* and *nrf* gene diversity analyses confirmed two pathways of nitrate attenuation by denitrification and DNRA. Furthermore, denitrification was identified as the primary nitrate reduction pathway in the LPS.

5. Conclusions

The combined use of hydrogeochemical, isotopic, and molecular biological analyses and laboratory flow-through experiments was applied to identify the occurrence of nitrate reduction and evaluate the nitrate reduction potential of LPS. The hydrochemical profile in the field site showed a close relationship between the hydrochemical composition and the mineralogy of the associated sediment. The redox zonation characterized by DO, ORP and reduced ions, appeared to be generally aligned with the sediment stratigraphy. FeO, MnO and FeS_2 were abundant in the LPS and acted as potential electron donors, contributing to the occurrence of chemolithotrophic denitrification.

The N, O, S isotopic profiles demonstrated strong bio-reduction of nitrate and sulfate in the HPS and LPS, particularly at the boundary between the aquifer and the LPS. The analyses of functional gene diversity (*nirS, nrf* and *dsr*) and isotopic compositions verified that the reductions in nitrate and sulfate were microbially mediated processes. The LPS has higher community diversity and bio-reduction potential than the HPS, as evidenced by the diversity indices (Shannon index, Chao1 and PD). The higher ratio of chemolithotrophs in the LPS than in the HPS revealed the adaptation of microbiological metabolisms to changes in the groundwater hydrochemistry. Due to the low level of nutrients in the anoxic LPS, chemolithotrophic denitrification and DNRA, in addition to heterotrophic denitrification, were the likely pathways contributing to nitrate attenuation.

Finally, the laboratory flow-through experiments of nitrate in the two sediment types demonstrated that the overall reduction rate was higher in the LPS than in the HPS. The measured reaction products NO_2^- and NH_4^+ verified the occurrence of denitrification and DNRA. This study provided evidence of the high reduction potential of LPS in aquifers. LPS could be an effective natural barrier attenuating high loads of nutrients, thereby protecting the underlying aquifers from contamination. Although the study addressed the significant contribution of chemolithotrophic denitrification, the ratio of chemolithotrophic/heterotrophic denitrification needs to be quantified. Furthermore, the in situ nitrate reduction rate of LPS is important for field predictions and merits future study.

Acknowledgements

This work was financially supported by the National Natural Science Foundation of China (No. 41501511, No. 41330632, and No. 41371121). We are grateful to Sun Yuqin, Sun Hui and Wang Yating for laboratory analyses and to Xiang Huang, Lu Xiangming and Mameng for their assistance with field sampling, and to three anonymous reviewers for their thoughtful comments that highly improved this paper.

Appendix A. Supplementary data

Supplementary data to this article can be found online at https://doi.org/10.1016/j.scitotenv.2017.11.039.

References

Akob, D.M., Kuesel, K., 2011. Where microorganisms meet rocks in the Earth's critical zone. Biogeosciences 8, 3531–3543.
An, S.M., Gardner, W.S., 2002. Dissimilatory nitrate reduction to ammonium (DNRA) as a nitrogen link, versus denitrification as a sink in a shallow estuary (Laguna Madre/Baffin Bay, Texas). Mar. Ecol. Prog. Ser. 237, 41–50.
Braker, G., Fesefeldt, A., Witzel, K.P., 1998. Development of PCR primer systems for amplification of nitrite reductase genes (nirK and nirS) to detect denitrifying bacteria in environmental samples. Appl. Environ. Microbiol. 64, 3769–3775.
Burgin, A.J., Hamilton, S.K., 2007. Have we overemphasized the role of denitrification in aquatic ecosystems? A review of nitrate removal pathways. Front. Ecol. Environ. 5, 89–96.
Caschetto, M., Colombani, N., Mastrocicco, M., Petitta, M., Aravena, R., 2017. Nitrogen and sulphur cycling in the saline coastal aquifer of Ferrara, Italy. A multi-isotope approach. Appl. Geochem. 76, 88–98.
Casciotti, K.L., Sigman, D.M., Hastings, M.G., Bohlke, J.K., Hilkert, A., 2002. Measurement of the oxygen isotopic composition of nitrate in seawater and freshwater using the denitrifier method. Anal. Chem. 74, 4905–4912.
Choi, B.-Y., Yun, S.-T., Mayer, B., Kim, K.-H., 2011. Sources and biogeochemical behavior of nitrate and sulfate in an alluvial aquifer: Hydrochemical and stable isotope approaches. Appl. Geochem. 26, 1249–1260.
Dragon, K., 2013. Groundwater nitrate pollution in the recharge zone of a regional Quaternary flow system (Wielkopolska region, Poland). Environ. Earth Sci. 68, 2099–2109.
Druhan, J.L., Bill, M., Lim, H., Wu, C., Conrad, M.E., Williams, K.H., DePaolo, D.J., Brodie, E.L., 2014. A large column analog experiment of stable isotope variations during reactive transport: II. Carbon mass balance, microbial community structure and predation. Geochim. Cosmochim. Acta 124, 394–409.
Einsiedl, F., Pilloni, G., Ruth-Anneser, B., Lueders, T., Griebler, C., 2015. Spatial distributions of sulphur species and sulphate-reducing bacteria provide insights into sulphur redox cycling and biodegradation hot-spots in a hydrocarbon-contaminated aquifer. Geochim. Cosmochim. Acta 156, 207–221.
Farhadian, M., Vachelard, C., Duchez, D., Larroche, C., 2008. In situ bioremediation of monoaromatic pollutants in groundwater: a review. Bioresour. Technol. 99, 5296–5308.
Feast, N.A., Hiscock, K.M., Dennis, P.F., Andrews, J.N., 1998. Nitrogen isotope hydrochemistry and denitrification within the Chalk aquifer system of north Norfolk, UK. J. Hydrol. 211, 233–252.
Flynn, T.M., O'Loughlin, E.J., Mishra, B., DiChristina, T.J., Kemner, K.M., 2014. Sulfur-mediated electron shuttling during bacterial iron reduction. Science 344, 1039–1042.
Green, C.T., Puckett, L.J., Bohlke, J.K., Bekins, B.A., Phillips, S.P., Kauffman, L.J., Denver, J.M., Johnson, H.M., 2008. Limited occurrence of denitrification in four shallow aquifers in agricultural areas of the United States. J. Environ. Qual. 37, 994–1009.
Guo, H., Yang, S., Tang, X., Li, Y., Shen, Z., 2008. Groundwater geochemistry and its implications for arsenic mobilization in shallow aquifers of the Hetao Basin, Inner Mongolia. Sci. Total Environ. 393, 131–144.
Guo, H., Zhou, Y., Jia, Y., Tang, X., Li, X., Shen, M., Lu, H., Han, S., Wei, C., Norra, S., Zhang, F., 2016. Sulfur cycling-related biogeochemical processes of arsenic mobilization in the Western Hetao Basin, China: evidence from multiple isotope approaches. Environ. Sci. Technol. 50, 12650–12659.
Hauck, S., Benz, M., Brune, A., Schink, B., 2001. Ferrous iron oxidation by denitrifying bacteria in profundal sediments of a deep lake (Lake Constance). FEMS Microbiol. Ecol. 37, 127–134.
Hemme, C.L., Green, S.J., Rishishwar, L., Prakash, O., Pettenato, A., Chakraborty, R., Deutschbauer, A.M., Van Nostrand, J.D., Wu, L., He, Z., Jordan, I.K., Hazen, T.C., Arkin,

A.P., Kostka, J.E., Zhou, J., 2016. Lateral gene transfer in a heavy metal-contaminated-groundwater microbial community. MBio 7 (2), e02234-15. https://doi.org/10.1128/mBio.02234-15.
Hendry, M.J., McCready, R.G.L., Gould, W.D., 1984. Distribution, source and evolution of nitrate in a glacial till of southern Alberta, Canada. J. Hydrol. 70, 177–198.
Herrmann, M., Rusznyak, A., Akob, D.M., Schulze, I., Opitz, S., Totsche, K.U., Kuesel, K., 2015. Large fractions of CO_2-fixing microorganisms in pristine limestone aquifers appear to be involved in the oxidation of reduced sulfur and nitrogen compounds. Appl. Environ. Microbiol. 81, 2384–2394.
Herrmann, M., Opitz, S., Harzer, R., Totsche, K.U., Kusel, K., 2017. Attached and suspended denitrifier communities in Pristine Limestone Aquifers Harbor high fractions of potential autotrophs oxidizing reduced iron and sulfur compounds. Microb. Ecol. 74 (2), 264–277.
Hill, A.R., Devito, K.J., Campagnolo, S., Sanmugadas, K., 2000. Subsurface denitrification in a forest riparian zone: interactions between hydrology and supplies of nitrate and organic carbon. Biogeochemistry 51, 193–223.
Hunkeler, D., Chollet, N., Pittet, X., Aravena, R., Cherry, J.A., Parker, B.L., 2004. Effect of source variability and transport processes on carbon isotope ratios of TCE and PCE in two sandy aquifers. J. Contam. Hydrol. 74, 265–282.
Kendall, C., 1998. Tracing nitrogen sources and cycling in catchments. In: Kendall, C., McDonnell, J. (Eds.), Isotope Tracers in Catchment Hydrology. Elsevier, Amsterdam, pp. 519–576.
Kendall, C., Elliott, E.M., Wankel, S.D., 2007. Tracing anthropogenic inputs of nitrogen to ecosystems. In: Michener, R., Lajtha, K. (Eds.), Stable Isotopes in Ecology and Environmental Science. Blackwell, pp. 375–449.
Khlebodarova, T.M., Ree, N.A., Likhoshvai, V.A., 2016. On the control mechanisms of the nitrite level in *Escherichia coli* cells: the mathematical model. BMC Microbiol. 16, 15–30.
Kim, H.S., Hur, S.J., 2017. Changes of sodium nitrate, nitrite, and *N*-nitrosodiethyiamine during in vitro human digestion. Food Chem. 225, 197–201.
Kim, K.H., Yun, S.T., Choi, B.Y., Chae, G.T., Joo, Y., Kim, K., Kim, H.S., 2009. Hydrochemical and multivariate statistical interpretations of spatial controls of nitrate concentrations in a shallow alluvial aquifer around oxbow lakes (Osong area, central Korea). J. Contam. Hydrol. 107, 114–127.
Kim, H., Kaown, D., Mayer, B., Lee, J.-Y., Hyun, Y., Lee, K.-K., 2015. Identifying the sources of nitrate contamination of groundwater in an agricultural area (Haean basin, Korea) using isotope and microbial community analyses. Sci. Total Environ. 533, 566–575.
Kleikemper, J., Schroth, M.H., Sigler, W.V., Schmucki, M., Bernasconi, S.M., Zeyer, J., 2002. Activity and diversity of sulfate-reducing bacteria in a petroleum hydrocarbon-contaminated aquifer. Appl. Environ. Microbiol. 68, 1516–1523.
Knoeller, K., Vogt, C., Feisthauer, S., Weise, S.M., Weiss, H., Richnow, H.-H., 2008. Sulfur cycling and biodegradation in contaminated aquifers: insights from stable isotope investigations. Environ. Sci. Technol. 42, 7807–7812.
Knoller, K., Strauch, G., 1999. Assessment of the flow dynamic of a mining lake by stable isotope investigations. Isot. Environ. Health Stud. 35, 75–83.
Korom, S.F., 1992. Natural denitrification in the saturated zone - a review. Water Resour. Res. 28, 1657–1668.
Li, L., Salehikhoo, F., Brantley, S.L., Heidari, P., 2014. Spatial zonation limits magnesite dissolution in porous media. Geochim. Cosmochim. Acta 126, 555–573.
Lima, G.d.P., Sleep, B.E., 2007. The spatial distribution of eubacteria and archaea in sand-clay columns degrading carbon tetrachloride and methanol. J. Contam. Hydrol. 94, 34–48.
Lovley, D.R., Phillips, E.J.P., 1994. Novel processes for anaerobic sulfate production from elemental sulfur by sulfate-reducing bacteria. Appl. Environ. Microbiol. 60, 2394–2399.
Lu, X., Cao, G., Huang, X., Clement, T.P., Zheng, C., 2016. Performance evaluation of inertial pumps used for sampling groundwater from small-diameter wells. Environ. Earth Sci. 75.
Ma, Z., Yang, Y., Lian, X., Jiang, Y., Xi, B., Peng, X., Yan, K., 2016. Identification of nitrate sources in groundwater using a stable isotope and 3DEEM in a landfill in Northeast China. Sci. Total Environ. 563, 593–599.
McMahon, P.B., 2001. Aquifer/aquitard interfaces: mixing zones that enhance biogeochemical reactions. Hydrogeol. J. 9, 34–43.
Mohan, S.B., Schmid, M., Jetten, M., Cole, J., 2004. Detection and widespread distribution of the nrfA gene encoding nitrite reduction to ammonia, a short circuit in the biological nitrogen cycle that competes with denitrification. FEMS Microbiol. Ecol. 49, 433–443.
Morasch, B., Richnow, H.H., Vieth, A., Schink, B., Meckenstock, R.U., 2004. Stable isotope fractionation caused by glycyl radical enzymes during bacterial degradation of aromatic compounds. Appl. Environ. Microbiol. 70, 2935–2940.
Noel, V., Boye, K., Kukkadapu, R.K., Bone, S., Pacheco, J.S.L., Cardarelli, E., Janot, N., Fendorf, S., Williams, K.H., Bargar, J.R., 2017. Understanding controls on redox processes in floodplain sediments of the Upper Colorado River Basin. Sci. Total Environ. 603, 663–675.
Nolan, B.T., Hitt, K.J., 2006. Vulnerability of shallow groundwater and drinking-water wells to nitrate in the United States. Environ. Sci. Technol. 40, 7834–7840.
Oh, H.-M., Kwon, K.K., Kang, I., Kang, S.G., Lee, J.-H., Kim, S.-J., Cho, J.-C., 2010. Complete genome sequence of "Candidatus Puniceispirillum marinum" IMCC1322, a representative of the SAR116 clade in the Alphaproteobacteria. J. Bacteriol. 192, 3240–3241.
Palau, J., Soler, A., Canals, A., Aravena, R., 2010. Use of environmental isotopes (13C, 15N, and 18O) for evaluating sources and fate of nitrate and Tetrachloroethene in an alluvial aquifer. Environ. Forensic 11, 237–247.
Rivett, M.O., Buss, S.R., Morgan, P., Smith, J.W.N., Bemment, C.D., 2008. Nitrate attenuation in groundwater: a review of biogeochemical controlling processes. Water Res. 42, 4215–4232.
Robertson, W.D., Russell, B.M., Cherry, J.A., 1996. Attenuation of nitrate in aquitard sediments of southern Ontario. J. Hydrol. 180, 267–281.
Rodvang, S.J., Simpkins, W.W., 2001. Agricultural contaminants in Quaternary aquitards: a review of occurrence and fate in North America. Hydrogeol. J. 9, 44–59.
Schaider, L.A., Rudel, R.A., Ackerman, J.M., Dunagan, S.C., Brody, J.G., 2014. Pharmaceuticals, perfluorosurfactants, and other organic wastewater compounds in public drinking water wells in a shallow sand and gravel aquifer. Sci. Total Environ. 468, 384–393.
Scheutz, C., Broholm, M.M., Durant, N.D., Weeth, E.B., Jorgensen, T.H., Dennis, P., Jacobsen, C.S., Cox, E.E., Chambon, J.C., Bjerg, P.L., 2010. Field evaluation of biological enhanced reductive dechlorination of Chloroethenes in clayey till. Environ. Sci. Technol. 44, 5134–5141.
Seitzinger, S., Harrison, J.A., Bohlke, J.K., Bouwman, A.F., Lowrance, R., Peterson, B., Tobias, C., Van Drecht, G., 2006. Denitrification across landscapes and waterscapes: a synthesis. Ecol. Appl. 16, 2064–2090.
Smith, R.L., Boehlke, J.K., Song, B., Tobias, C.R., 2015. Role of anaerobic ammonium oxidation (Anammox) in nitrogen removal from a freshwater aquifer. Environ. Sci. Technol. 49, 12169–12177.
Stoewer, M.M., Knoeller, K., Stumpp, C., 2015. Tracing freshwater nitrate sources in prealpine groundwater catchments using environmental tracers. J. Hydrol. 524, 753–767.
Straub, K.L., Benz, M., Schink, B., Widdel, F., 1996. Anaerobic, nitrate-dependent microbial oxidation of ferrous iron. Appl. Environ. Microbiol. 62, 1458–1460.
Suzuki, D., Li, Z., Cui, X., Zhang, C., Katayama, A., 2014. Reclassification of *Desulfobacterium anilini* as *Desulfatiglans anilini* comb. nov within *Desulfatiglans* gen. nov., and description of a 4-chlorophenol-degrading sulfate-reducing bacterium, *Desulfatiglans parachlorophenolica* sp. nov. Int. J. Syst. Evol. Microbiol. 64, 3081–3086.
Wang, Y., 2014. Migration and Transformation of Nitrate in the Aquitard: Experimental and Modeling Studies. (Master). Peking University, Beijing.
Wanner, P., Parker, B.L., Chapman, S.W., Aravena, R., Hunkeler, D., 2016. Quantification of degradation of chlorinated hydrocarbons in saturated low permeability sediments using compound-specific isotope analysis. Environ. Sci. Technol. 50, 5622–5630.
White, R.A., Rivett, M.O., Tellam, J.H., 2008. Paleo-roothole facilitated transport of aromatic hydrocarbons through a Holocene clay bed. Environ. Sci. Technol. 42, 7118–7124.
Xu, C., Li, Y., Li, Q., Dong, Y., Fang, F., Guo, Z., 2013. Measurement of N-15 and O-18 isotope abundance of nitrate using denitrifier method on tracegas-isotope ratio mass spectrometry. In: Zhao, J., Iranpour, R., Li, X., Jin, B. (Eds.), Advances in Environmental Technologies. Pts 1–6. 726–731, pp. 1346–1349.
Xue, D., Botte, J., De Baets, B., Accoe, F., Nestler, A., Taylor, P., Van Cleemput, O., Berglund, M., Boeckx, P., 2009. Present limitations and future prospects of stable isotope methods for nitrate source identification in surface- and groundwater. Water Res. 43, 1159–1170.
Yan, S., Liu, Y., Liu, C., Shi, L., Shang, J., Shan, H., Zachara, J., Fredrickson, J., Kennedy, D., Resch, C.T., Thompson, C., Fansler, S., 2016. Nitrate bioreduction in redox-variable low permeability sediments. Sci. Total Environ. 539, 185–195.
Zein, M.M., Suidan, M.T., Venosa, A.D., 2004. MtBE biodegradation in a gravity flow, high-biomass retaining bioreactor. Environ. Sci. Technol. 38, 3449–3456.
Zhang, Y.C., Slomp, C.P., Broers, H.P., Passier, H.F., Van Cappellen, P., 2009. Denitrification coupled to pyrite oxidation and changes in groundwater quality in a shallow sandy aquifer. Geochim. Cosmochim. Acta 73, 6716–6726.
Zhang, D., Li, X.-D., Zhao, Z.-Q., Liu, C.-Q., 2015. Using dual isotopic data to track the sources and behaviors of dissolved sulfate in the western North China Plain. Appl. Geochem. 52, 43–56.
Zhu, G., Xia, C., Shanyun, W., Zhou, L., Liu, L., Zhao, S., 2015. Occurrence, activity and contribution of anammox in some freshwater extreme environments. Environ. Microbiol. Rep. 7, 961–969.